Spontaneous and superfluid chiral edge states in exciton-polariton condensates

H. Sigurdsson,[1,*] G. Li,[2] and T. C. H. Liew[3]

[1]*Science Institute, University of Iceland, Dunhagi-3, IS-107 Reykjavik, Iceland*

[2]*School of Physics and Astronomy, University of Southampton, Southampton SO17 1BJ, United Kingdom*

[3]*Division of Physics and Applied Physics, School of Physical and Mathematical Sciences, Nanyang Technological University, 21 Nanyang Link, Singapore 637371*

(Received 10 July 2017; revised manuscript received 18 September 2017; published 29 September 2017)

We present a scheme of interaction-induced topological band structures based on the spin anisotropy of exciton-polaritons in semiconductor microcavities. We predict theoretically that this scheme allows the engineering of topological gaps, without requiring a magnetic field or strong spin-orbit interaction (transverse electric-transverse magnetic splitting). Under nonresonant pumping we find that an initially topologically trivial system undergoes a topological transition upon the spontaneous breaking of phase symmetry associated with polariton condensation. Under either nonresonant or resonant coherent pumping we find that it is also possible to engineer a topological dispersion that is linear in wave vector—a property associated with polariton superfluidity.

DOI: 10.1103/PhysRevB.96.115453

I. INTRODUCTION

The hybridization of light and matter in the form of exciton-polaritons in microcavities has led to a new kind of quantum fluid [1], well known for its ability to develop coherence spontaneously as a Bose-Einstein condensate [2,3] and flow without friction as a superfluid [4,5], even at room temperature [6]. Furthermore, it has been shown that exciton-polaritons can be manipulated by highly tunable optically induced potentials [7,8]. These allow introducing a spatial structure in an otherwise homogeneous system, which has given access to a variety of fundamental effects, including: the gating [9,10] and routing [11,12] of polariton flow, the trapping of polariton superfluids [13,14], the formation of patterns [15], the breaking of chiral symmetry [16], and the exposure of exceptional points [17].

Taking inspiration from the field of topological photonics [18], recent theoretical works have considered engineering topological polariton band structures [19–22]. These are characterized by the formation of chiral edge states, at the boundaries between areas with different topology, which exhibit unidirectional propagation and an absence of backscattering even in the presence of defects or disorder. Due to these properties, chiral edge states are highly relevant to the field of polaritonics, which seeks robust mechanisms of propagating fields between individual information processing elements to allow for cascadable systems [23–25]. The presence of Kerr-type interactions between polaritons would also allow the development of a nonlinear topological photonics, where schemes for solitons forming in the chiral edge modes have also appeared in recent theoretical works [26–28].

Previous schemes of topological polaritons have been based on three ingredients. First, a periodic potential is required to introduce the band structure on which to impose nontrivial topology. This has implicated the need for hard engineering of the polariton potential, achieved by, e.g., etching micropillar arrays [29]. Second, so that edge states propagate in only one direction, time-reversal symmetry should be broken, which implies the application of a magnetic field. Third, a significant amount of spin-orbit coupling is needed, which implies strong transverse electric-transverse magnetic (TE-TM) splitting. While large TE-TM splitting (on the order of tenths of milli-electronvolts) was achieved in samples from decades ago [30], microcavities have evolved over the years to reduce this splitting (the quality factor is optimum when the cavity mode frequency is at the center of the stop band, where the TE-TM splitting is smallest). Even though the aforementioned three ingredients can be achieved in principle, we will show that actually none of them are essential for generating topological polaritons!

We will consider a planar microcavity (with no etching), corresponding to an initially topologically trivial system, and illumination by a spatially patterned optical field, strong enough to place polaritons in a nonlinear regime. We find that the spin anisotropy of polariton-polariton interactions induces an effective spin-orbit coupling and breaking of time-reversal symmetry. In contrast to the trivial time-reversal symmetry breaking of typical dissipative systems, this form allows the creation of nontrivial topology. Remarkably, since these effects depend on the polariton interaction energy (blueshift), we obtain topological gaps that exceed typical strengths of disorder. The effect is readily observable making use of polarization filtering to separate the injected condensate and the topological behavior.

Aside from the interest that topological photonics brings to polaritonics, there is also a question of whether or not exciton-polaritons can bring anything new to the field of topological photonics? It is well established that under nonresonant pumping polaritons must achieve their coherence spontaneously. Consequently the topological behavior that arises from an initially trivial system is also developed spontaneously, where a random choice of the system chirality determines in which way chiral edge states will propagate. Under either nonresonant or resonant pumping we also find that it is possible to obtain a topological dispersion that is linear in the wave vector (in the case of resonant pumping this however requires an additional potential). A linear dispersion is generally considered a sufficient condition for polariton superfluidity [1,31,32]. As far as we know, these are unique features that do not appear in other topological photonic systems.

*Corresponding author: helg@hi.is

 ©2017 American Physical Society

II. THEORETICAL MODEL

We begin by defining the wave functions of polaritons in the x and y linear in-plane polarizations as ψ_x and ψ_y, respectively. Their evolution is determined by the polarization dependent driven-dissipative Gross-Pitaevskii equations [32]

$$i\hbar\frac{\partial\psi_{x,y}}{\partial t} = \Big[E_{x,y} - \frac{\hbar^2}{2m}\nabla^2 - \frac{i\Gamma_{x,y}}{2} + V(\mathbf{x}) + iP(\mathbf{x}) + (U_0 - i\Gamma_{\rm NL})(|\psi_x|^2 + |\psi_y|^2)\Big]\psi_{x,y} - U_1\big(|\psi_{x,y}|^2\psi_{x,y} + \psi_{y,x}^2\psi_{x,y}^*\big) + F_{x,y}(\mathbf{x})e^{-i\omega_p t}. \quad (1)$$

Here the equations are written in a general form, allowing for different energies (polarization splitting) of the x and y components, E_x and E_y, respectively, and different lifetimes, Γ_x and Γ_y, respectively. The effective polariton mass m and potential $V(\mathbf{x})$ are polarization independent. We account for the potential term here for generality, being interested in both spatially homogeneous and etched microcavities. The nonlinear polariton-polariton interaction constants are related to those in the spinor basis [33] by $U_0 = \alpha_1$ and $U_1 = (\alpha_1 - \alpha_2)/2$. It is well established that typically α_2 is negative, while α_1 is positive and that $|\alpha_2| \leqslant |\alpha_1|$ [34,35]. The nonlinear loss terms $\Gamma_{\rm NL}$ are most relevant when considering nonresonant pumping [36]. Experiments on spin bifurcations, where a polariton condensate suddenly becomes macroscopically spin polarized under linear polarized excitation, have been fitted assuming that the nonlinear loss rate is polarization independent and that $\Gamma_x \neq \Gamma_y$ and $E_x \neq E_y$ [37].

III. EXCITATION SCHEMES

In the following we will consider different mechanisms of driving the system: (1) nonresonant excitation, for which $F_{x,y}(\mathbf{x}) = 0$ and the potential term should be supplemented by a pump-induced shift [38], $V(\mathbf{x}) = gP(\mathbf{x})$, where g is a dimensionless constant; and (2) resonant x-linearly polarized excitation, for which $\Gamma_{\rm NL} \approx 0$, $P(\mathbf{x}) = 0$, $F_y(\mathbf{x}) = 0$, and ω_p is the pump frequency. In either case we can expect the polariton condensate to be polarized in the x direction. Under resonant pumping this is obvious due to direct injection of x-polarized polaritons. Under nonresonant pumping, polariton condensates are also typically linearly polarized in microcavities where there is a polarization splitting [39]. This is modeled by allowing $\Gamma_x \neq \Gamma_y$. If $\Gamma_x < \Gamma_y$, then the condensation threshold belongs to an x-polarized condensate.

For simplicity, we now consider the case $U_0 = U_1 = \alpha$, which is consistent with experimental measurements in Refs. [40,41]. In this limit driving of the x polarization does not excite significantly the y polarization. Setting $\psi_y = 0$ decouples the equation for evolution of the x-polarized component:

$$i\hbar\frac{\partial\psi_x}{\partial t} = \Big(E_x - \frac{\hbar^2}{2m}\nabla^2 - \frac{i\Gamma_x}{2} + V(\mathbf{x}) + iP(\mathbf{x}) - i\Gamma_{\rm NL}|\psi_x|^2\Big)\psi_x + F_x(\mathbf{x})e^{-i\omega_p t}. \quad (2)$$

Note that the U_0 and U_1 dependent terms involving $|\psi_x|^2$ have been canceled.

We will take the driving fields to have a lattice type structure, where $F_{x,y}(\mathbf{x})$ and $P_{x,y}(\mathbf{x})$ are periodic in the x direction with periodicity a. It is then appropriate to take a as the natural unit of length and $\epsilon = \hbar^2/(2ma^2)$ as the natural unit of energy. With these choices, Eq. (2) can be rescaled to take the form

$$i\frac{\partial\psi_x'}{\partial t'} = \Big(E_x' - \hbar\omega_p' - \nabla'^2 - \frac{i\Gamma_x'}{2} + V'(\mathbf{x}) + iP'(\mathbf{x}) - i|\psi_x'|^2\Big)\psi_x' + F_x'(\mathbf{x}), \quad (3)$$

where $\psi_x' = \sqrt{\Gamma_{\rm NL}/\epsilon}\,\psi_x\exp(-i\omega_p t)$, $t' = \epsilon t/\hbar$, $x' = x/a$, $y' = y/a$, $F_x' = F_x\sqrt{\Gamma_{\rm NL}}/\epsilon^{3/2}$, and all other primed parameters are scaled by ϵ (e.g., $E_{x,y}' = E_{x,y}/\epsilon$). By rescaling the equations we show that the results are reproducible over a large parameter range.

IV. DISPERSION

While the effective mass characterizes the dispersion of polaritons in the low-density regime, under the build-up of significant polariton populations the dispersion becomes renormalized [31,42–44]. Let us focus our attention on the dispersion of y-polarized polaritons, which evolve under the scaled evolution equation:

$$i\frac{\partial\psi_y'}{\partial t'} = \Big(E_y' - \hbar\omega_p' - \nabla'^2 - \frac{i\Gamma_y'}{2} + V'(\mathbf{x}) + iP'(\mathbf{x}) - i|\psi_x'|^2 + \alpha'|\psi_x'|^2\Big)\psi_y' - \alpha'\psi_x'^2\psi_y'^*, \quad (4)$$

where $\alpha'|\psi_x'|^2 = \alpha|\psi_x|^2/\epsilon$ (or equivalently $\alpha' = \alpha/\Gamma_{\rm NL}$) and we continue working in the regime where the occupation of ψ_y is small.

Due to the last term in Eq. (4) the dispersion of the y-polarized polaritons should be calculated by substituting a form $\psi_y' = A_{k_x}(\mathbf{x})e^{i\omega t} + B_{k_x}(\mathbf{x})e^{-i\omega^* t}$, where $A_{k_x}(\mathbf{x})$ and $B_{k_x}(\mathbf{x})$ are the wave-vector dependent Bloch envelope functions accounting for the periodicity a. We note that the problem is not PT symmetric and that the eigenvalues are complex. The positive and negative frequency components are coupled upon substitution into Eq. (4) and we obtain two coupled equations, which can be written in matrix form:

$$\begin{pmatrix} E' & -\alpha'\psi_x'^2 \\ \alpha'\psi_x'^{*2} & -E'^* \end{pmatrix}\begin{pmatrix} A_{k_x}(\mathbf{x}) \\ B_{k_x}(\mathbf{x}) \end{pmatrix} = \hbar\omega'\begin{pmatrix} A_{k_x}(\mathbf{x}) \\ B_{k_x}(\mathbf{x}) \end{pmatrix}, \quad (5)$$

where

$$E' = -\nabla'^2 + E_y' - E_p' - \frac{i\Gamma_y'}{2} + (\alpha' - i)|\psi_x'|^2 + V'(\mathbf{x}) + iP'(\mathbf{x}). \quad (6)$$

Here, E_p' is the energy of the ψ_x' polaritons either given by the frequency of the pump (resonant case) or the chemical potential of the ψ_x' condensate (nonresonant case).

The complex eigenvalues $\hbar\omega'$ of Eq. (5) determine the energy spectrum. Having written the equations for generic

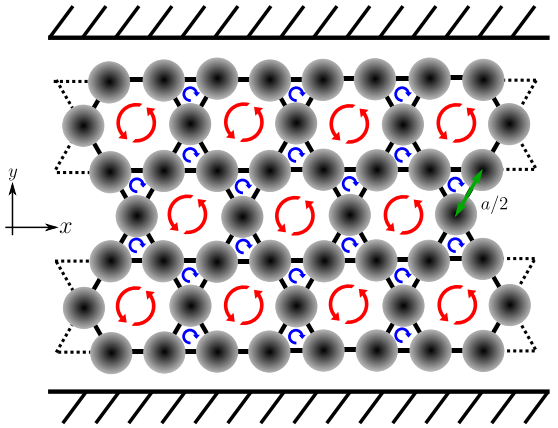

FIG. 1. A kagome lattice of Gaussian pump spots (gray) in the nonresonant excitation scheme. We choose the lattice to be periodic in the x direction but finite in the y direction enforced with a hard wall potential. Tuning the width and distance between the spots we find that a stable vortex lattice forms spontaneously with periodic arrangement of charge ± 2 (red) and ∓ 1 (blue) vortices. Here we set $a = 16\ \mu$m and FWHM of the spots to $\sigma' = 0.31$.

driving of the system, either nonresonant or resonant, we will focus separately on these two cases in the following.

V. NONRESONANT PUMPING

For a given lattice to generate a topological dispersion (in the opposite polarization component), we require it to contain plaquettes of nonzero flux. We find that the kagome lattice of vortices is the simplest lattice compatible with both nonresonant pumping and topological dispersion. Several experimental [45,46] and theoretical studies [36,47] have considered the generation of vortex-antivortex lattices, their stability [48], and the phase locking of vortices [49,50]. Here we find that nonresonant excitation with an intensity pattern corresponding to a kagome lattice spontaneously forms a lattice of vortices in phase (see Fig. 1 for a graphical representation of the excitation scheme and subsequent vortex formation). Setting $\Gamma_y > \Gamma_x$ and slowly ramping the pump intensity produces the x-polarized condensate.

In contrast to chiral pumping schemes [16], our pumping field is nonchiral, such that the handedness of the vortices (that is, the sign of their winding number) is spontaneously chosen. All properties derived from the handedness of the vortices, such as an emergent nontrivial topology, are thus also spontaneously developed.

Given ψ_x, the calculation of the dispersion of the y-polarized field follows from Eq. (5) and application of the Bloch theory. We consider a strip geometry which is infinite in the x direction, but with finite size in the y direction. In Fig. 2(a) we plot the real part of the eigenvalues $\hbar\omega'$ belonging only to stable states characterized by $\mathrm{Im}(\omega) \leqslant 0$ (zero or negative Lyapunov components). We find a clear signature of topologically protected edges states in the ψ_y component separated by bulk bands (blue). Here green lines correspond to the upper edge of the condensate and red to the lower edge. The coloring changes continuously to blue as the localization of the state goes away from the edges into the bulk. We point

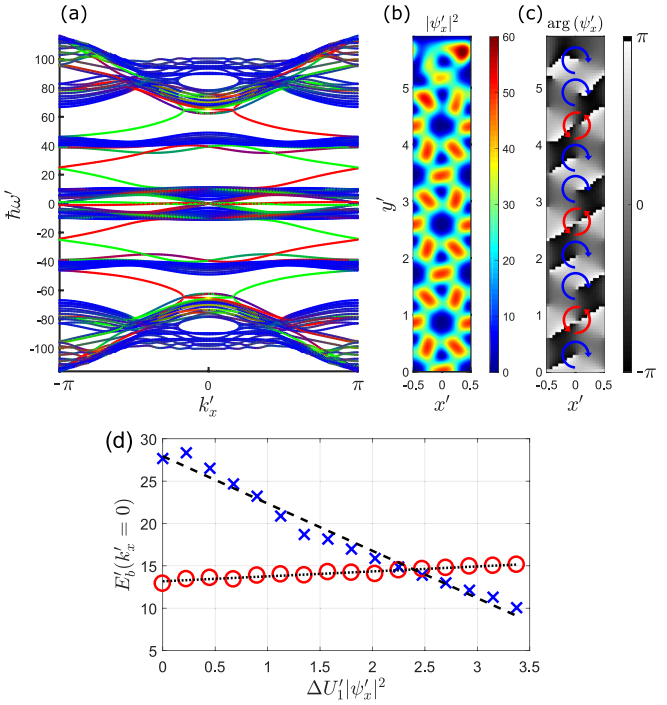

FIG. 2. (a) Bogoliubov spectrum of the nonresonantly driven polariton condensate in a strip geometry. The rotation of the vortex lattice in the condensate sets the topology of different bulk bands (blue) which are bridged by green (red) chiral edge states on the upper (lower) edge. The coloring changes continuously to blue as the localization of the state goes away from the edges into the bulk. (b) Density of the condensate vortex lattice in the upper half the of strip. (c) Phase of the condensate. Red double arrows indicate charge 2 vortices, whereas blue single arrows charge -1 vortices. (d) Change in the band gaps from (a) as a function of deviation in spin interaction strength ($U'_1 = \alpha' - \Delta U'_1$). Blue crosses are lower band gap and red circles upper band gap. Black dashed and dotted lines are a guide to the eye. Parameters were set to: $a = 16\ \mu$m, $m = 5 \times 10^{-5} m_0$, $\Gamma'_x = 22$, $\Gamma'_y = 33$, $E_{x,y} = 0$, $\alpha' = 8.8$, $g = 0.6$, and $P' \approx 88$, where P' is the pump profile maximum. $E'_p \approx 83$ is set by the chemical potential of the ψ_x condensate.

out that it is important that the linewidth corresponding to the imaginary part is smaller than the topological bandwidth in the real part. Figures 2(b) and 2(c) shows the steady state in the ψ_x component.

The observed topological band gap has a size on the order of 30ϵ. In real units, a typical polariton mass $m = 5 \times 10^{-5} m_0$, where m_0 is the mass of a free electron, and a typical lattice constant $a = 16\ \mu$m sets an energy scale $\epsilon = 3\ \mu$eV. The typical topological gap size is then on the order of 0.09 meV, which exceeds the decay rate and typical strengths of disorder in modern samples. The experimental observation of the band gap requires $\alpha'|\psi'_x|^2 \approx 450$. Typically this would correspond to a 1.35 meV nonlinear shift, which is routinely observed in experiments [8–10]. Another requirement would be a polariton linewidth smaller than the band gap size, i.e., less than $30\epsilon = 0.09$ meV. Such linewidths are also readily available in modern microcavity samples [8–10,51], and even linewidths in the μeV range have been reported [52]. In Fig. 2(d) we show the dependence of the the band gaps size (E_b) from Fig. 2(a),

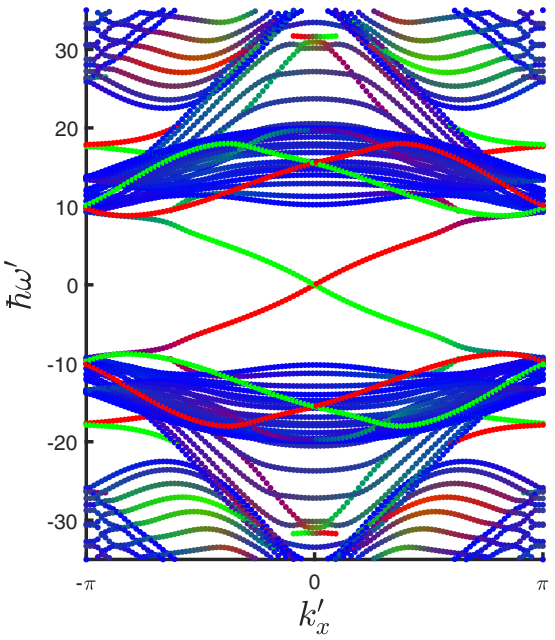

FIG. 3. Another example of the Bogoliubov spectrum of the nonresonantly driven polariton condensate in a strip geometry showing possible superfluid edge states connecting the bands. Parameters were set to: $a = 16\ \mu$m, $m = 5 \times 10^{-5} m_0$, $\Gamma'_x = 22$, $\Gamma'_y = 28$, $E'_x = 0$, $E'_y = 7$, $\alpha' = 4.8$, $g = 0.6$, and $P' \approx 88$, where P' is the pump profile maximum. $E'_p \approx 83$ is set by the chemical potential of the ψ_x condensate.

measured at $k'_x = 0$, as a function of interaction strength $U'_1 = \alpha' - \Delta U'_1$. The deviation $\Delta U'_1$ is set as positive corresponding to $|\alpha_2| \leqslant |\alpha_1|$. Blue crosses correspond to the lower band gap and red circles the upper band gap. One sees that the gaps display different behavior with the lower one closing fast and the upper opening slowly, indicating that the topology of the system is not necessarily lost when $U_0 \neq U_1$.

The presence of a hard-wall (Dirichlet) boundary at the edges of the strip in the y' direction causes a static deformation of the x component of the condensate at the edges but does not destabilize the lattice. In the current scheme where $\psi'_y \sim 0$ the vortex lattice is stable over a long time scale ($t \sim 10^2$ ns) with zero net interactions due to the cancellation between the U_0 and U_1 terms allowing us to freely play with α when resolving the Bogoliubov dispersion. We note that $\psi'_y \sim 0$ is only stable as long as fluctuations within it will not grow. This can be controlled by tuning the splitting $E'_{x,y}$ and/or $\Gamma'_{x,y}$. In the case of an imbalance between U_0 and U_1, we have also found stable vortex-antivortex lattices, however there are limitations to their intensity as the vortices can become unstable with increasing pumping power [49].

In order to stress the variety of edge states possible in the nonresonantly driven system, we show a nearly linear edge state dispersion connecting the bulk bands (see Fig. 3). It has been pointed out by several theoretical works in exciton-polariton systems that, due to the Landau criterion, a linear in k dispersion corresponds to the phenomenon of superfluidity [1,31,32,53]. The phenomenon was reported by several experimental works [4–6], but never in the presence of a nontrivial topology. The traditional method of distinguishing superfluidity in polariton systems, which is based on observing a suppression of scattering with a defect, might not be considered sufficient in our system as the topological protection of the chiral edge state already prevents scattering with disorder. We expect that topological polariton superfluids should be characterized by their linear dispersion.

VI. RESONANT PUMPING

Under resonant pumping, the phase of an incident optical field can be imprinted onto the polariton field, giving a more direct control. We consider a stationary polariton field in the x polarization of the form

$$\psi_x(\mathbf{x}) = \psi_0 e^{-i\omega_p t} \sum_{n=1}^{6} e^{i(\mathbf{k}_n \cdot \mathbf{x} + \phi_n)}, \tag{7}$$

where ψ_0 defines the amplitude; the wave vectors are $\mathbf{k}_{1,2} = k_0(\pm\sqrt{3}/2, 1/2)$, $\mathbf{k}_{3,4} = k_0(0, \pm 1)$, and $\mathbf{k}_{5,6} = k_0(\pm\sqrt{3}/2, -1/2)$, where $k_0 = 4\pi/(\sqrt{3}a)$; and the phase factors are $\phi_{1,2,3,4} = 0$ and $\phi_{5,6} = \pm 2\pi/3$. This form corresponds to a kagome vortex-antivortex, with the same phenomenology as shown in Fig. 1.

Under resonant pumping, the terms $P(\mathbf{x})$ and Γ_{NL} are typically neglected in the modeling of exciton-polariton systems since it is common to assume that there is no reservoir of hot excitons (as excitons with energy above the pump energy are unlikely to be excited) and consequently there is no gain saturation or nonlinear loss [31,32]. Under such conditions, it is straightforward to show that the field $\psi_x(\mathbf{x})$ can be imprinted by a specific choice of the pumping field, which is given by substituting the form of Eq. (7) into Eq. (3) and solving for $F_x(\mathbf{x})$. In practice, the dispersion term has little effect and the pumping field will take an analogous form to $\psi_x(\mathbf{x})$, that is, it will be composed primarily by six different wave vector components [54].

The dispersion of the y component is then obtained from application of the Bloch theory, giving the result shown in Fig. 4. As before, we only plot the real part of the dispersion

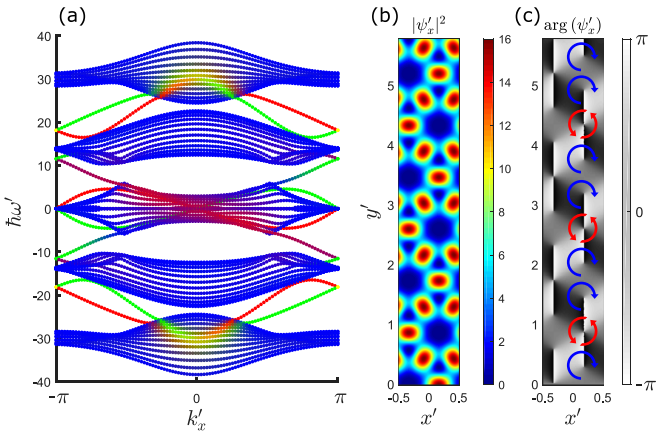

FIG. 4. (a) Optically induced topological dispersion under resonant coherent pumping. (b) Density of the condensate vortex lattice in the upper half the of strip. (c) Phase of the condensate. Red double arrows indicate charge 2 vortices, whereas blue single arrows charge −1 vortices. Parameters: $\Gamma'_{x,y} = 0.5$, $E'_{x,y} = 0, \alpha'|\psi'_x|^2 = 160$, $E'_p = 41$, $V' = 0$, $P(\mathbf{x}) = 0$, $\Gamma_{\mathrm{NL}} = 0$.

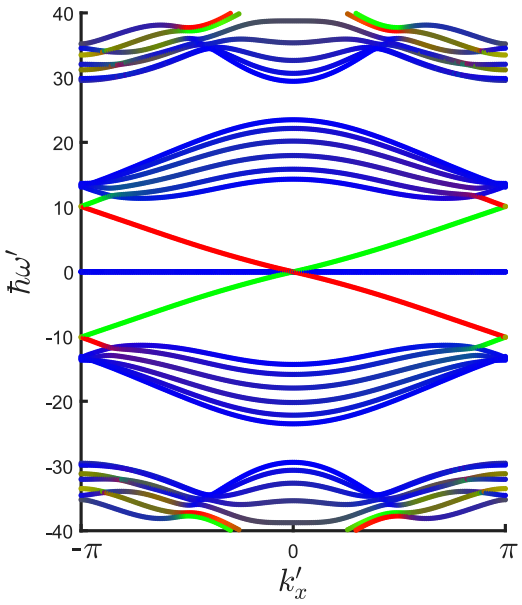

FIG. 5. Optically induced topological dispersion under resonant coherent pumping and kagome lattice potential $V(\mathbf{x})$. The ψ_x condensate is the same as in Figs. 4(b) and 4(c). Parameters: $\Gamma'_{x,y} = 0.5$, $E'_{x,y} = 0$, $\alpha'|\psi'_x|^2 = 96$, $E'_p = 0$, $V'(\mathbf{x}) = -\alpha'|\psi_x|^2$, $P(\mathbf{x}) = 0$, $\Gamma_{\mathrm{NL}} = 0$.

corresponding to stable states. One sees a clear gap in the dispersion, where bulk states do not appear. The gap is topological, being bridged by a pair of chiral edge states that are localized on opposite edges of the strip.

This scheme may appear similar to that considered in Ref. [55], which was based on a similar equation to Eq. (5), but the context and interpretation is very different. Indeed we rely on interactions to introduce a form of synthetic magnetism (artificial gauge field) [56], but we are making strong use of the polarization dependence of the interactions, which was not considered before in this context to our knowledge. By exciting a field with one linear polarization (x), we find that topological behavior appears in the opposite linear polarization (y). It should be noted that the dispersion of y-polarized polaritons can be distinguished from the more highly populated x polarization using polarization filtering. In addition, since the problem has been effectively divided into two parts, that is, solution of the x-polarized field from Eq. (3), and the dispersion of the y-polarized field from Eq. (5), it becomes easier to find parameters that give a topological band gap. In particular the dispersion shown in Fig. 4 depends on the scaled parameter $\alpha'|\psi'_x|^2 = 160$ and shows a topological gap of typical size $\sim 5\epsilon$.

While topological behavior is obtained in the case $V(\mathbf{x}) = 0$, it is still interesting to consider the case when there is an additional potential patterning of the microcavity. For simplicity, we assume that the potential is etched also in the form of a kagome lattice $V'(\mathbf{x}) = -\alpha'|\psi_x|^2$. We find that this allows the dispersion of the y-polarized component to not only be topological but, again, also linear in k, as shown in Fig. 5, and similar to the nonresonant case in Fig. 3. While a specific potential is needed for the resonant superfluid case, we stress that the topological behavior is compatible with different potential shapes (including zero potential as illustrated in Fig. 4).

VII. CONCLUSION

We have introduced schemes of optically induced topological polaritons, characterized by the formation of chiral edge states, making use of the action of a condensate in one linear polarization on the dispersion of polaritons in the other. The scheme is compatible with unetched planar microcavities and does not require any significant spin-orbit coupling (TE-TM splitting) in the sample or applied magnetic field.

Under nonresonant excitation, the phase orientation of a vortex-antivortex (kagome) lattice is spontaneously chosen and responsible for the topological behavior. Exciton-polaritons thus exhibit a unique feature among topological photonic systems, where an initially topologically trivial state undergoes a spontaneous topological phase transition with spontaneously chosen chirality. Under resonant excitation, the topological dispersion can be obtained, also with no external potential present. Special cases for both nonresonant and resonant excitation schemes reveal edge state dispersions linear in k, representative of a polariton superfluid.

ACKNOWLEDGMENTS

H.S. acknowledges support by the Research Fund of the University of Iceland, The Icelandic Research Fund, Grant No. 163082-051. G.L. acknowledges the EPSRC Programme on Hybrid Polaritonics for financial support. T.L. acknowledges support from the Ministry of Education (Singapore) Grant 2015-T2-1-055.

[1] I. Carusotto and C. Ciuti, Rev. Mod. Phys. **85**, 299 (2013).
[2] J. Kasprzak, M. Richard, S. Kundermann, A. Baas, P. Jeambrun, J. M. J. Keeling, F. M. Marchetti, M. H. Szymanska, R. Andre, J. L. Staehli, V. Savona, P. B. Littlewood, B. Deveaud, and L. S. Dang, Nature (London) **443**, 409 (2006).
[3] T. Byrnes, N. Y. Kim, and Y. Yamamoto, Nat. Phys. **10**, 803 (2014).
[4] A. Amo, J. Lefrere, S. Pigeon, C. Adrados, C. Ciuti, I. Carusotto, R. Houdre, E. Giacobino, and A. Bramati, Nat. Phys. **5**, 805 (2009).
[5] D. Sanvitto, F. M. Marchetti, M. H. Szymanska, G. Tosi, M. Baudisch, F. P. Laussy, D. N. Krizhanovskii, M. S. Skolnick, L. Marrucci, A. Lemaitre, J. Bloch, C. Tejedor, and L. Vina, Nat. Phys. **6**, 527 (2010).
[6] G. Lerario, A. Fieramosca, F. Barachati, D. Ballarini, K. S. Daskalakis, L. Dominici, M. De Giorgi, S. A. Maier, G. Gigli, S. Kéna-Cohen, and D. Sanvitto, Nat. Phys. **13**, 837 (2017).
[7] A. Amo, S. Pigeon, C. Adrados, R. Houdré, E. Giacobino, C. Ciuti, and A. Bramati, Phys. Rev. B **82**, 081301 (2010).
[8] E. Wertz, A. Amo, D. D. Solnyshkov, L. Ferrier, T. C. H. Liew, D. Sanvitto, P. Senellart, I. Sagnes, A. Lemaître, A. V. Kavokin, G. Malpuech, and J. Bloch, Phys. Rev. Lett. **109**, 216404 (2012).

[9] T. Gao, P. S. Eldridge, T. C. H. Liew, S. I. Tsintzos, G. Stavrinidis, G. Deligeorgis, Z. Hatzopoulos, and P. G. Savvidis, Phys. Rev. B **85**, 235102 (2012).

[10] C. Antón, T. C. H. Liew, J. Cuadra, M. D. Martín, P. S. Eldridge, Z. Hatzopoulos, G. Stavrinidis, P. G. Savvidis, and L. Viña, Phys. Rev. B **88**, 245307 (2013).

[11] H. Flayac and I. G. Savenko, Appl. Phys. Lett. **103**, 201105 (2013).

[12] F. Marsault, H. S. Nguyen, D. Tanese, A. Lemaître, E. Galopin, I. Sagnes, A. Amo, and J. Bloch, Appl. Phys. Lett. **107**, 201115 (2015).

[13] G. Tosi, G. Christmann, N. G. Berloff, P. Tsotsis, T. Gao, Z. Hatzopoulos, P. G. Savvidis, and J. J. Baumberg, Nat. Phys. **8**, 190 (2012).

[14] P. Cristofolini, A. Dreismann, G. Christmann, G. Franchetti, N. G. Berloff, P. Tsotsis, Z. Hatzopoulos, P. G. Savvidis, and J. J. Baumberg, Phys. Rev. Lett. **110**, 186403 (2013).

[15] F. Manni, K. G. Lagoudakis, T. C. H. Liew, R. André, and B. Deveaud-Plédran, Phys. Rev. Lett. **107**, 106401 (2011).

[16] R. Dall, M. D. Fraser, A. S. Desyatnikov, G. Li, S. Brodbeck, M. Kamp, C. Schneider, S. Höfling, and E. A. Ostrovskaya, Phys. Rev. Lett. **113**, 200404 (2014).

[17] T. Gao, E. Estrecho, K. Y. Bliokh, T. C. H. Liew, M. D. Fraser, S. Brodbeck, M. Kamp, C. Schneider, S. Hofling, Y. Yamamoto, F. Nori, Y. S. Kivshar, A. G. Truscott, R. G. Dall, and E. A. Ostrovskaya, Nature (London) **526**, 554 (2015).

[18] L. Lu, J. D. Joannopoulos, and M. Soljacic, Nat. Photon. **8**, 821 (2014).

[19] T. Karzig, C.-E. Bardyn, N. H. Lindner, and G. Refael, Phys. Rev. X **5**, 031001 (2015).

[20] C.-E. Bardyn, T. Karzig, G. Refael, and T. C. H. Liew, Phys. Rev. B **91**, 161413 (2015).

[21] A. V. Nalitov, D. D. Solnyshkov, and G. Malpuech, Phys. Rev. Lett. **114**, 116401 (2015).

[22] K. Yi and T. Karzig, Phys. Rev. B **93**, 104303 (2016).

[23] D. Ballarini, M. De Giorgi, E. Cancellieri, R. Houdré, E. Giacobino, R. Cingolani, A. Bramati, G. Gigli, and D. Sanvitto, Nat. Commun. **4**, 1778 (2013).

[24] T. Espinosa-Ortega and T. C. H. Liew, Phys. Rev. B **87**, 195305 (2013).

[25] D. Sanvitto and S. Kena-Cohen, Nat. Mater. **15**, 1061 (2016).

[26] D. Leykam and Y. D. Chong, Phys. Rev. Lett. **117**, 143901 (2016).

[27] Y. V. Kartashov and D. V. Skryabin, Optica **3**, 1228 (2016).

[28] D. R. Gulevich, D. Yudin, D. V. Skryabin, I. V. Iorsh, and I. A. Shelykh, Sci. Rep. **7**, 1780 (2017).

[29] M. Milićević, T. Ozawa, P. Andreakou, I. Carusotto, T. Jacqmin, E. Galopin, A. Lemaître, L. L. Gratiet, I. Sagnes, J. Bloch, and A. Amo, 2D Mater. **2**, 034012 (2015).

[30] G. Panzarini, L. C. Andreani, A. Armitage, D. Baxter, M. S. Skolnick, V. N. Astratov, J. S. Roberts, A. V. Kavokin, M. R. Vladimirova, and M. A. Kaliteevski, Phys. Rev. B **59**, 5082 (1999).

[31] I. Carusotto and C. Ciuti, Phys. Rev. Lett. **93**, 166401 (2004).

[32] I. A. Shelykh, Y. G. Rubo, G. Malpuech, D. D. Solnyshkov, and A. Kavokin, Phys. Rev. Lett. **97**, 066402 (2006).

[33] I. A. Shelykh, A. V. Kavokin, Y. G. Rubo, T. C. H. Liew, and G. Malpuech, Semicond. Sci. Technol. **25**, 013001 (2010).

[34] D. N. Krizhanovskii, D. Sanvitto, I. A. Shelykh, M. M. Glazov, G. Malpuech, D. D. Solnyshkov, A. Kavokin, S. Ceccarelli, M. S. Skolnick, and J. S. Roberts, Phys. Rev. B **73**, 073303 (2006).

[35] C. Leyder, T. C. H. Liew, A. V. Kavokin, I. A. Shelykh, M. Romanelli, J. P. Karr, E. Giacobino, and A. Bramati, Phys. Rev. Lett. **99**, 196402 (2007).

[36] J. Keeling and N. G. Berloff, Phys. Rev. Lett. **100**, 250401 (2008).

[37] H. Ohadi, A. Dreismann, Y. G. Rubo, F. Pinsker, Y. del Valle-Inclan Redondo, S. I. Tsintzos, Z. Hatzopoulos, P. G. Savvidis, and J. J. Baumberg, Phys. Rev. X **5**, 031002 (2015).

[38] M. Wouters and I. Carusotto, Phys. Rev. Lett. **99**, 140402 (2007).

[39] J. Kasprzak, R. André, L. S. Dang, I. A. Shelykh, A. V. Kavokin, Y. G. Rubo, K. V. Kavokin, and G. Malpuech, Phys. Rev. B **75**, 045326 (2007).

[40] M. Vladimirova, S. Cronenberger, D. Scalbert, K. V. Kavokin, A. Miard, A. Lemaître, J. Bloch, D. Solnyshkov, G. Malpuech, and A. V. Kavokin, Phys. Rev. B **82**, 075301 (2010).

[41] N. Takemura, S. Trebaol, M. Wouters, M. T. Portella-Oberli, and B. Deveaud, Phys. Rev. B **90**, 195307 (2014).

[42] S. Utsunomiya, L. Tian, G. Roumpos, C. W. Lai, N. Kumada, T. Fujisawa, M. Kuwata-Gonokami, A. Loffler, S. Hofling, A. Forchel, and Y. Yamamoto, Nat. Phys. **4**, 700 (2008).

[43] V. Kohnle, Y. Léger, M. Wouters, M. Richard, M. T. Portella-Oberli, and B. Deveaud-Plédran, Phys. Rev. Lett. **106**, 255302 (2011).

[44] M. Pieczarka, M. Syperek, L. Dusanowski, J. Misiewicz, F. Langer, A. Forchel, M. Kamp, C. Schneider, S. Höfling, A. Kavokin, and G. Sęk, Phys. Rev. Lett. **115**, 186401 (2015).

[45] G. Tosi, G. Christmann, N. G. Berloff, P. Tsotsis, T. Gao, Z. Hatzopoulos, P. G. Savvidis, and J. J. Baumberg, Nat. Commun. **3**, 1243 (2012).

[46] T. Boulier, E. Cancellieri, N. D. Sangouard, R. Hivet, Q. Glorieux, É. Giacobino, and A. Bramati, C. R. Phys. **17**, 893 (2016).

[47] A. S. Rodrigues, P. G. Kevrekidis, R. Carretero-González, J. Cuevas-Maraver, D. J. Frantzeskakis, and F. Palmero, J. Phys.: Condens. Matter **26**, 155801 (2014).

[48] X. Ma, O. A. Egorov, and S. Schumacher, Phys. Rev. Lett. **118**, 157401 (2017).

[49] H. Sigurdsson, O. A. Egorov, X. Ma, I. A. Shelykh, and T. C. H. Liew, Phys. Rev. B **90**, 014504 (2014).

[50] X. Ma and S. Schumacher, Phys. Rev. B **95**, 235301 (2017).

[51] T. Gao, G. Li, E. Estrecho, T. C. H. Liew, D. Comber-Todd, A. Nalitov, M. Steger, K. West, L. Pfeiffer, D. Snoke, A. V. Kavokin, A. G. Truscott, and E. A. Ostrovskaya, arXiv:1705.09752.

[52] Y. Sun, P. Wen, Y. Yoon, G. Liu, M. Steger, L. N. Pfeiffer, K. West, D. W. Snoke, and K. A. Nelson, Phys. Rev. Lett. **118**, 016602 (2017).

[53] E. Cancellieri, F. M. Marchetti, M. H. Szymańska, D. Sanvitto, and C. Tejedor, Phys. Rev. Lett. **108**, 065301 (2012).

[54] T. C. H. Liew, Y. G. Rubo, and A. V. Kavokin, Phys. Rev. Lett. **101**, 187401 (2008).

[55] C.-E. Bardyn, T. Karzig, G. Refael, and T. C. H. Liew, Phys. Rev. B **93**, 020502 (2016).

[56] N. Westerberg, C. Maitland, D. Faccio, K. Wilson, P. Öhberg, and E. M. Wright, Phys. Rev. A **94**, 023805 (2016).